ELSEVIER

Polymer 40 (1999) 2587–2594

polymer

Influence of the morphology and of the supermolecular structure on the enzymatic degradation of bacterial poly(3-hydroxybutyrate)

M. Canetti*, M. Urso, P. Sadocco

Stazione Sperimentale Cellulosa, Carta e Fibre Tessili Vegetali ed Artificiali, P.zza Leonardo da Vinci 26, I-20133 Milan, Italy

Received 3 February 1998; revised 16 June 1998; accepted 16 June 1998

Abstract

Films of poly(3-hydroxybutyrate) (PHB) were crystallized from the melt by different thermal treatments and submitted to enzymatic degradation by using a PHB depolymerase purified from *Aureobacterium saperdae* culture. The morphology and the supermolecular structure of PHB films were investigated to explain differences in the kinetics of enzymatic degradation. Differential scanning calorimetry, optical microscopy, wide-angle X-ray diffraction and small-angle X-ray scattering were employed to characterize the PHB films. A decreasing of enzymatic degradation rate was observed with the increasing of crystallinity and crystal dimension of the PHB films. PHB samples showing the same degree of crystallinity and similar value of lamellar thickness were prepared using different isothermal crystallization and annealing temperatures. The differences in the enzymatic degradation rate of these films were explained in terms of morphological parameters.

Keywords: Poly(3-hydroxybutyrate); Enzymatic degradation; Structural characterization

1. Introduction

Poly (D(-)3-hydroxybutyrate) (PHB) is accumulated by a wide variety of micro-organisms as an intracellular storage source of organic carbon and chemical energy. PHB has attracted much attention as a biocompatible and biodegradable thermoplastic polymer with potential application in agricultural, medical and marine fields [1].

Studies of enzymatic degradation of bacterial PHB single crystals by different extracellular PHB depolymerases indicated preferential degradation from the crystal edge rather than the chain folds of the lamellar surface. The results gave elucidation on the degradation mechanism, and suggested that both endo and exo mechanism of enzymatic degradation could be involved in the process [2–6]. However, single crystals of PHB have a unique folded chain lamellar structure, while in the case of semi-crystalline PHB films the morphology and the supermolecular structure can play an important role on the kinetic of enzymatic degradation of PHB.

Kumagai et al. [7] reported that the rate of enzymatic degradation of PHB film by a PHB depolymerase from *Alcaligenes feacalis* is strongly influenced by the degree of crystallinity, but it is less dependent on the size of PHB spherulites. Tomasi et al. [8] reported that the rate of enzymatic hydrolysis of PHB film decreases with increasing crystal size and that morphological changes affect the rate of enzymatic degradation for films where the degree of crystallinity is kept constant. Recently, the different rates of enzymatic degradation of PHB films, isothermally crystallized from the melt at different temperatures, were mainly attributed to different crystal sizes when the crystallinity values of the films were similar [9].

In the present work the PHB depolymerase from *Aureobacterium saperdae* is used to investigate the effect of the supermolecular structure and of the morphology on the rate of enzymatic degradation of PHB film. The thermal treatment reserved for the samples was chosen to prepare films with similar morphology or supermolecular structure but different biodegradation behavior.

2. Experimental

2.1. Materials

The bacterial PHB used in this study was a semi-crystalline polymer isolated from *Alcaligenes eutrophus* cultures (Zeneca Bioproducts; $M_w = 166\,000$, $M_w/M_n = 2.85$). Thin films of PHB were prepared by the solution-casting technique

* Corresponding author. Tel.: +39-2-23-95531; Fax: +39-2-23-65039; E-mail: sscctlib@icil64.cilea.it

0032-3861/99/$ - see front matter
PII: S0032-3861(98)00503-5

Table 1
Sample preparation

Sample code	Thermal treatment
C50	Isothermal crystallization at 50°C for 7 min
A100	Isothermal crystallization at 50°C for 7 min followed by annealing at 100°C for 30 min
C100	Isothermal crystallization at 100°C for 30 min
A130	Cooling from the melt (185°C) to 130°C at 0.5°C/min followed by annealing at 130°C for 96 h

from dichloromethane solutions of the polymer, using glass Petri dishes as casting surfaces. The PHB films were melted at 185°C for 2 min in a small oven and immediately transferred in an automatic hot-stage Mettler model FP-82 controlled by a Mettler FP-80 control processor for the thermal treatments reported in Table 1.

2.2. Enzymatic degradation

Enzymatic degradation of PHB films was carried out using a PHB depolymerase purified from *Aureobacterium saperdae* culture [10]. PHB films (initial dimensions: 10 × 10 mm; initial weight: about 20 mg), were placed in vials containing 2.0 ml of potassium phosphate buffer (100 mM, pH 7.0) and 15 μg of PHB depolymerase. The reaction solution was incubated at 37 ± 0.1°C with gentle shaking. After 20 h the samples were removed from the solutions, washed with distilled water and dried to constant weight in vacuum. In experiments lasting several days, this procedure was repeated using fresh enzymatic solution for each 20 h incubation interval. Control experiments were carried out without the addition of the depolymerase. The enzymatic degradation results are reported as the weight loss divided by the sample surface area. The weight loss data were averaged on three film samples.

2.3. Differential scanning calorimetry

The overall kinetics of crystallization of the PHB were analyzed by using a Perkin-Elmer DSC-4 with a Perkin-Elmer 3600 Data Station (TADS System). The rate of heat evolution during the isothermal crystallization was recorded as a function of time starting on samples melted at 185°C for 2 min and rapidly cooled to the desired crystallization temperature, T_c. The weight fraction, X_t, of the polymer crystallized at the time t was calculated using the relation

$$X_t = \frac{\int_0^t (\mathrm{d}H/\mathrm{d}t)\mathrm{d}t}{\int_0^\infty (\mathrm{d}H/\mathrm{d}t)\mathrm{d}t} \quad (1)$$

where the first integral is the heat generated at time t and the second is the total heat when crystallization is complete. The half-time of crystallization $t_{0.5}$ is the time taken for half of the crystallinity to develop. The kinetic data were also analyzed by using the Avrami equation [11]

$$X_t = 1 - \exp(-K_n t^n) \quad (2)$$

where n is a parameter depending on the geometry of the growing crystals and on the nucleation process and K_n is the overall kinetic rate constant. Indium standard samples was employed to calibrate the temperature scale and the heat of transition.

2.4. Optical microscopy

The morphology and the spherulite growth rate of PHB film were studied using an optical polarizing microscope equipped with an automatic hot stage, Mettler model FP82, controlled by a Mettler FP80 control processor.

2.5. Wide-angle X-ray diffraction

X-ray diffraction measurements were obtained at room temperature using a Siemens diffractometer model D-500 equipped with a Siemens FK 60-10, 2000 W Cu tube (CuK_α radiation, $\lambda = 1.54$ Å). The degree of crystallinity by weight, ω, was calculated from diffracted intensity data in the range $2\Theta = 5$–$50°$ by using the area integration method [12]. The amorphous contribution was obtained from the diffracted intensity data of PHB quenched in an ice–water mixture, at the measuring temperature of 3°C. The degree of crystallinity by volume, ϕ, was calculated by

$$\phi = 1/\left(1 + \frac{1-\omega}{\omega}\frac{\rho_c}{\rho_a}\right) \quad (3)$$

were for the amorphous density a value of $\rho_a = 1.177$ g/cm^3 was assumed [13], and the crystal density ρ_c was determined as described below.

The orthorombic cell parameters were optimized by a least-square fit procedure [14] starting from the experimental 2θ angular position of the reflections and using the cell parameters reported by Okamura and Marchessault [15] as reference. From the calculated volume of the unit cell, and by assuming four monomeric units per unit cell, the ρ_c value of 1.270 g/cm^3 was evaluated in good agreement with the value reported by Yochouki et al. [16].

The apparent crystal size $D_{(020)}$ of PHB in the direction perpendicular to the 020 crystallographic plane was calculated

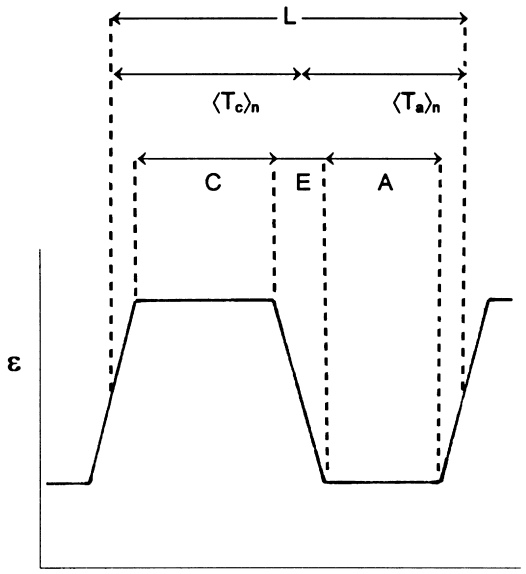

Fig. 1. Electron density (ε) profile in a direction perpendicular to the lamellae for a pseudo two phase model.

from the line-broadening data by applying the Scherrer equation [12]

$$D_{(020)} = \frac{K\lambda}{\beta_0 \cos\theta} \tag{4}$$

where β_0 is the half width in radians of the reflections corrected for instrumental broadening. The shape factor K is set equal to unity, and so the size have to be considered as relative data. A nickel standard sample was employed to determine the instrumental broadening.

2.6. Small-angle X-ray scattering

The SAXS measurements were conducted at 21°C with a Kratky Compact Camera. Monocromatized CuK_α radiation ($\lambda = 1.54$ Å) were supplied by a stabilized Siemens Krystalloflex 710 generator and a Siemens FK 60-04, 1500 W Cu target tube operated at 40 kV and 25 mA. The scattered intensity was counted for 600 s at 140 angles of measurement in the range $2\theta = 0.1$–$3.6°$, by using a step scanning proportional counter with pulse height discrimination. The blank scattering was subtracted from the sample scattering after correction for the sample absorption to obtain the intensity value $\bar{I}$. For all the SAXS measurement the abscissa variable was $s = (2/\lambda)\sin\theta$. After subtraction of the continuous background scattering [17], the desmearing procedure was applied [18]. The one-dimensional scattering function $I_1(s) = 4\pi s^2 I(s)$, corresponding to the scattering profile of lamellar stacks perpendicular to the layer, was obtained from the desmearing scattering function $I(s)$, using the Lorentz correction. The periodicity L was calculated by applying Bragg's law to the scattering maximum in the Lorentz plot (I_1 vs s).

The experimental scattering data were also analyzed considering the pseudo-two-phase model [19]. The model can be defined as consisting of alternating parallel amorphous and crystalline lamellae connected by transition layer (E), which can be represented as a linear variation of the electron density between the crystalline and amorphous cores C and A respectively (Fig. 1). The tail region of the scattering intensity can be approximated by

$$\bar{I}(s) = (\pi k/2)[1/s^3 - 2\pi^2 E^2/(3s)] \tag{5}$$

where k is a constant and E is the transition layer thickness, which can be evaluate by plotting $s\bar{I}(s)$ vs $1/s^2$ [19].

The number average lamellar thickness $\langle T_c \rangle_n$ can be determined from the one-dimensional correlation function

$$\gamma_1(x) = \int_0^\infty s\bar{I}(s)[J_0(2\pi xs) - (2\pi xs)J_1(2\pi xs)]\mathrm{d}s \Big/ \int_0^\infty s\bar{I}(s)\mathrm{d}s \tag{6}$$

where J_0 and J_1 are the zero and the first-order Bessel functions and x is the direction of lamellar stacking.

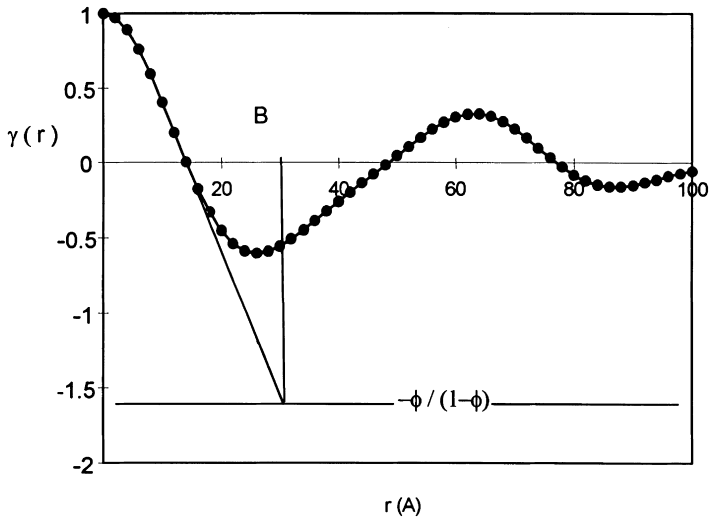

Fig. 2. One-dimensional correlation function: sample A100.

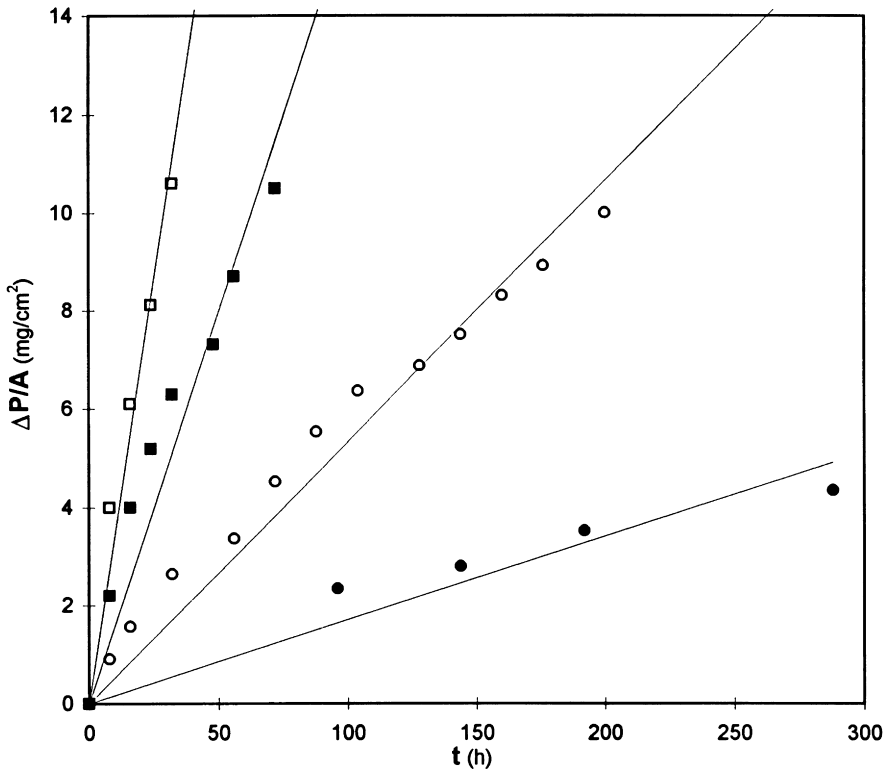

Fig. 3. Kinetics of enzymatic degradation of PHB films: □, C50; ■, A100; ○, C100; ●, A130.

A typical one-dimensional correlation function is reported in Fig. 2, where the horizontal baseline was constructed at $-\phi/(1-\phi)$. $\langle T_c\rangle_n$ was calculated from the relation [17]

$$\langle T_c\rangle_n = B + E\phi/3(1-\phi) \quad (7)$$

where B is the projection on the x axis of the intercept of the tangent to the linear region of $\gamma_1(x)$ with the horizontal baseline. Analogously, the number average amorphous thickness, $\langle T_a\rangle_n$, was calculated from the relation

$$\langle T_a\rangle_n = B + E(1-\phi)/3\phi \quad (8)$$

In this case the horizontal baseline to extrapolate the B value was constructed at $-(1-\phi)/\phi$.

The one-dimensional correlation function of the A130 sample showed a horizontal region in the first minimum that can be associated with the amorphous volume fraction [20] and allow the direct calculation of the $\langle T_c\rangle_n$ and $\langle T_a\rangle_n$ values (see Fig. 8).

The crystalline and amorphous core thicknesses C and A were calculated by

$$C = \langle T_c\rangle_n - E,\ A = \langle T_a\rangle_n - E \quad (9)$$

Processing of the small-angle X-ray scattering data was done with the FFSAXS-5 program [21].

3. Results and discussion

3.1. Enzymatic degradation

The PHB enzymatic degradation results, expressed as weight loss divided by sample surface area, are reported in Fig. 3. The average rate of enzymatic degradation (S), calculated from the kinetics data are reported in Table 2. The curves and the relative S values show strong dependence on sample thermal history. The annealing at 100°C of the sample isothermally crystallized at 50°C produced an increasing of the resistance to the biodegradation. However, the A100 sample shows an enzymatic degradation rate higher than the C100 sample isothermally crystallized at 100°C from the melt. The thermal condition adopted to prepare the A130 sample, determined a drastic reduction of the enzymatic degradation rate.

Table 2
Average rate of enzymatic degradation (S), degree of crystallinity by weight (ω), apparent crystal size ($D_{(020)}$)

PHB sample	S (mg/cm^{2}h)	ω	$D_{(020)}$ (Å)
C50	0.314	0.51	345
A100	0.136	0.64	385
C100	0.049	0.64	430
A130	0.018	0.76	790

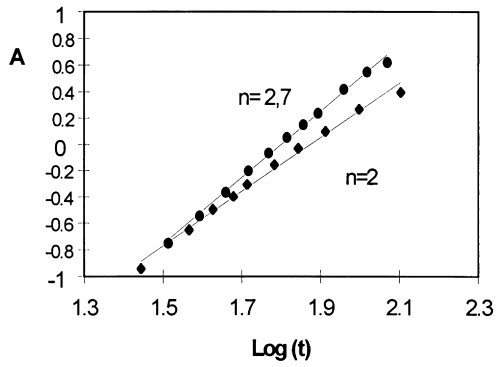

Fig. 4. Avrami plot of C50 (●) and C100 (♦) samples. $A = \mathrm{Log}[-\ln(1 - X_t)]$.

3.2. Thermal characterization and morphology

The overall rate of crystallization of a supercooled liquid is determined by the rate of formation of nuclei above the critical size, and by the growth rate of such nuclei to the final crystalline aggregates. The overall kinetics of crystallization of the PHB were obtained from DSC at the crystallization temperatures of 50 and 100°C; the calculated half-time of crystallization of PHB was similar for both T_c: 55 and 60 s, respectively. The optical microscopy investigations showed that the nucleation rate of PHB isothermally crystallized from the melt at 50°C was higher (ten times) than PHB crystallized at 100°C. Spherulitic growth rate values of 25 and 200 μm/min were observed for PHB crystallized at the temperatures of 50 and 100°C, respectively. The nucleation and spherulitic growth rate data are in good agreement with the data reported in literature [22–24]. Therefore, the C50 and C100 samples reached the complete crystallization in about the same time but through two different crystallization processes in terms of nucleation and transport factors, as also suggested by the analysis of the isothermal bulk crystallization kinetic data by using the Avrami approach. For the C50 and C100 samples the values of n were determined from the slope, of straight lines obtained by plotting $\mathrm{Log}[-\ln(1 - Xt)]$ vs $\mathrm{Log}\, t$ (Fig. 4). The value of the Avrami exponent, n, was equal to 2 for the C100 sample in agreement with Dubini-Paglia et al. [25], while a non-integral value of n equal to 2.7 was observed for the C50 sample.

The morphologies of C50 and C100 samples were quite different. In fact, when observed by optical microscopy, the C100 sample showed spherulites with an average radius of 1 mm, while spherulite radii from 20 to 50 μm were observed for the C50 sample (Fig. 5). The A100 sample was prepared by annealing treatment of C50 sample to reach the degree of crystallinity of the C100 sample (Table 2). The spherulitic morphology of A100 sample was unchanged with respect to the C50 sample. Spherulites with a radius of 2–3 mm were measured for the A130 sample.

3.3. Wide-angle X-ray diffraction

The diffraction profiles of PHB samples reported in Fig. 6 are a first indication of the difference in the PHB structure due to the adopted crystallization conditions. For the A50 and C100 samples, differences in the ratio of the peak intensity were observed with respect to the C100, A130 samples. The diffraction profiles of the C50 and A100 samples were generally less resolved compared with the samples crystallized at higher temperatures, while the diffraction peak at $2\theta = 17°$ relative to the (110) crystallographic plane appeared more pronounced. The intensity of the reflections at $2\theta = 13.3°$ relative to the (020) crystallographic plane and at $2\theta = 26.8°$ relative to the (040) crystallographic plane increases by annealing and by increasing the crystallization temperature. The peak positions remain practically unchanged for all the investigated samples.

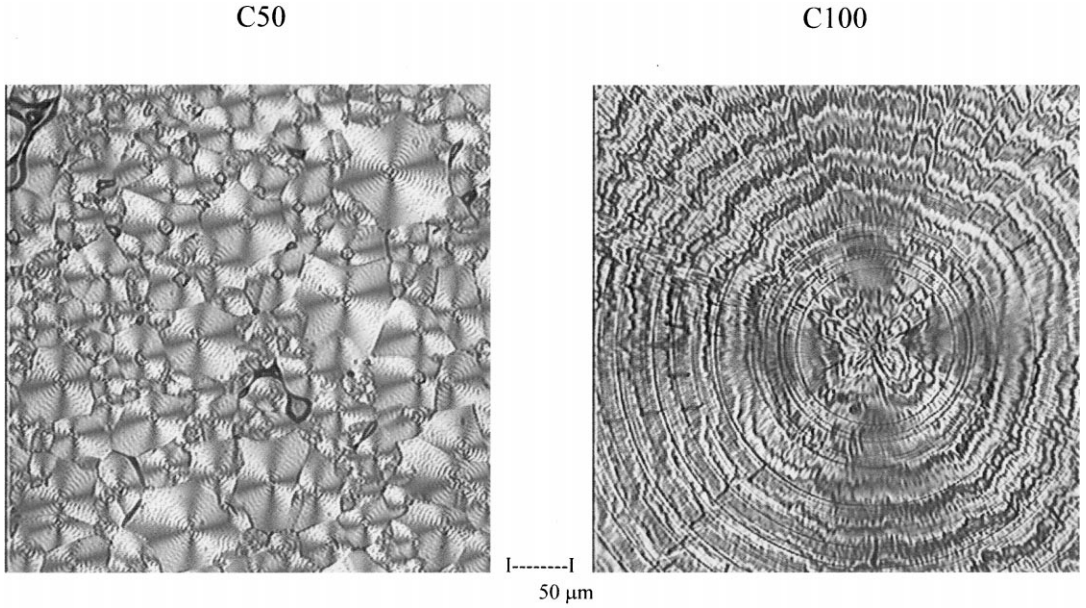

Fig. 5. Light micrographs of PHB films: C50 and C100.

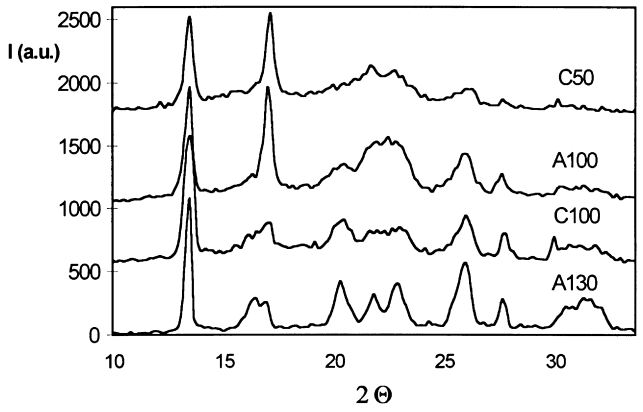

Fig. 6. Wide-angle X-ray diffraction profiles of PHB films: C50, A100, C100, A130.

Gazzano et al. [26] attributed differences in the ratio of the peak intensity to the different degrees of orientation of the crystalline lamellae parallel to the film plane due to the differences in the spherulite size in films of limited thickness. In fact in the present work, the adopted crystallization temperatures strongly influenced the spherulite size.

The values of the degree of crystallinity by weight, ω, are reported in Table 2. It is known that the rate of enzymatic degradation of PHB can be strongly influenced by crystallinity [7]. However, the rates of enzymatic degradation S (Table 2) for the A100 and C100 samples were significantly different in spite of the same degree of crystallinity values.

The annealing of the PHB sample isothermally crystallized at 50°C produced the increase in the apparent crystal size, $D_{(020)}$. Anyway, the $D_{(020)}$ value of the A100 sample resulted to be smaller than the $D_{(020)}$ value calculated for the C100 sample. The crystallization condition reserved for the A130 sample produced a drastic increase in the apparent crystal dimension (Table 2).

3.4. Small-angle X-ray scattering

The scattering profile of the PHB samples showed the presence of a maximum, that is associated with the periodicity L, resulting from the presence of macrolattice formed by centres of adjacent lamellae. From the maximum of the Lorentz-corrected intensity profiles (Fig. 7) the weight-average values of periodicity, L_w, were calculated and reported in Table 3. As a consequence of the annealing treatment, the A100 sample showed a L_w value higher than the C50 sample. The thermal treatment induced the same crystallinity degree for A100 and C100 samples, the observed different L_w values are a first indication of differences in the sample structures. The A130 sample showed the higher L_w value as consequence of the drastic thermal treatment.

The one-dimensional correlation function plots showed a pronounced maximum for all samples, indicative of a regular stacking of the lamellae. From the positions of the first positive maximum the number-average value of periodicity L_n, were calculated and reported in Table 3. The agreement between the L_w and L_n values is an indication of the low polydispersity of the periodicity for all samples [17,27].

The correlation functions and the bulk volume crystallinities (ϕ) were combined to give the average thicknesses $\langle T \rangle_n$, according to the pseudo-two-phase model. The obtained values of C and A (Table 3) are the same for the C100 and A100 samples, then the difference between the L_n values should be ascribed to the difference in the transition layer E. However, the standard deviation of E and $\langle T \rangle_n$ values (estimated from 2 to 3 Å and obtained by the variation of volume crystallinity and background correction) does not allow a meaningful differentiation between the samples. The C50 sample showed minor lamellar thickening.

The one-dimensional correlation function calculated for

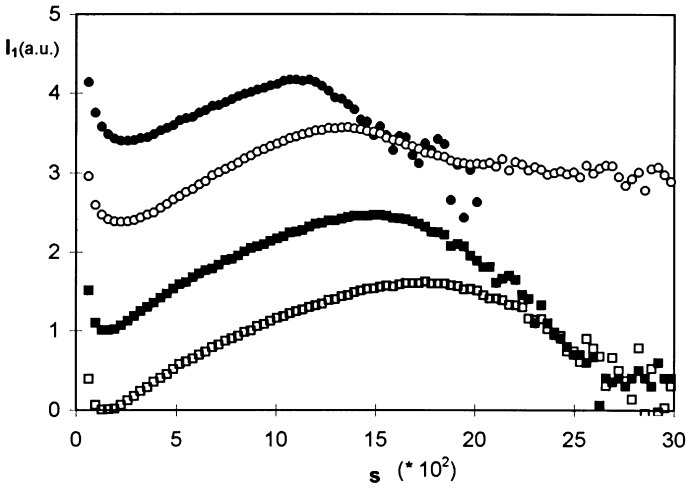

Fig. 7. One-dimensional scattering function obtained by Lorentz correction: □, C50; ■, A100; ○, C100; ●, A130.

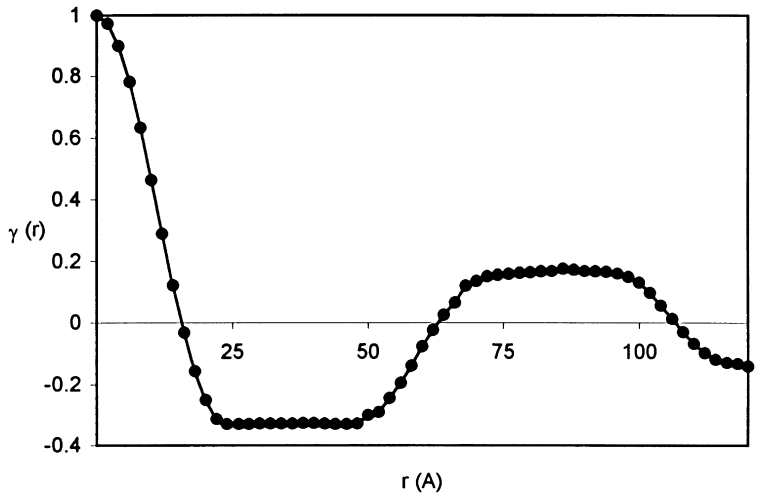

Fig. 8. One-dimensional correlation function: sample A130.

the A130 sample, showed a horizontal region in the first minimum allowing the direct extrapolation of the structural parameters (Fig. 8). The deduced volume crystallinity was very close to the ones calculated by WAXD data (Table 3). The thermal condition adopted to prepare the A130 sample induced an increasing of the lamellar core thickness that results to be twofold with respect to the sample crystallized or annealed at 100°C.

4. Conclusions

The annealing at 100°C of PHB films isothermally crystallized at 50°C produced an increase in crystallinity and crystal dimension values and a resulting decrease in enzymatic degradation rate. The relative high resistance to the biodegradation observed for the A130 sample is justified by the high value of the considered crystalline parameters and by the low number of spherulites per unit surface.

The A100 and C100 samples showed a significantly different enzymatic degradation rate, in spite of very similar supermolecular parameters (ω, C and A). Kumagai et al. [7] reported that the rate of enzymatic degradation of PHB film is dependent on the crystallinity but independent of the size of spherulites. Tomasi et al. [8] reported for films of PHB at a constant degree of crystallinity that the rate of enzymatic hydrolysis is influenced by spherulite and crystal sizes. In the case of A100 and C100 samples the thermal treatment chosen produced different morphology in term of number of spherulites per unit surface. The higher rate of biodegradation of the A100 sample with respect to the C100 sample can be explained mainly by the presence of large number of spherulite core and of spherulites impinging fronts that are subjected to preferential enzymatic degradation [8]. In fact, in our opinion the observed difference between the two samples in term of crystal dimension D_{020}, is not sufficient to explain the large difference in the rate of enzymatic degradation.

References

[1] Doi Y. Microbial polyesters. New York: VCH, 1990.
[2] Hocking PJ, Marchessault RH, Timmins MR, Scherer TM, Lenz RW, Fuller RC. Macromol Rapid Commun 1994;15:447.
[3] Hocking PJ, Timmins MR, Scherer TM, Lenz RW, Fuller RC, Marchessault RH. J Macromol Sci Pure Appl Chem 1995;A32:889.
[4] Timmins MR, Lenz RW, Hocking PJ, Marchessault RH, Fuller RC. Macromol Chem Phys 1996;197:1193.
[5] Hocking PJ, Marchessault RH, Timmins MR, Lenz RW, Fuller RC. Macromolecules 1996;29:2472.
[6] Iwata T, Doi Y, Kasuya K, Inoue Y. Macromolecules 1997;30:833.
[7] Kumagai Y, Kanesawa Y, Doi Y. Makromol Chem 1992;193:53.
[8] Tomasi G, Scandola M, Briese BH, Jendrossek D. Macromolecules 1996;29:507.
[9] Koyama N, Doi Y. Macromolecules 1997;30:826.

Table 3
Weight-average values of periodicity (L_w), crystallinity by volume (ϕ), number-average value of periodicity (L_n), number average lamellar and amorphous thicknesses, $\langle T_c \rangle_n$ and $\langle T_a \rangle_n$, transition layer, crystalline and amorphous core thicknesses, E, C and A

Sample	L_w	ϕ	L_n (Å)	E (Å)	$\langle T_c \rangle_n$ (Å)	C (Å)	$\langle T_a \rangle_n$ (Å)	A (Å)
C50	53	0.49	54	16	28	12	26	10
A100	62	0.62	62	14	39	25	22	8
C100	68	0.62	68	18	42	25	25	8
A130	85	0.75[a]	83	11	58	47	25	14
		0.74						

[a]By SAXS.

[10] Sadocco P, Nocerino S, Dubini-Paglia E, Seves A, Elegir G. J Environ Polym Degrad 1997;5:57.
[11] Avrami MJ. J Chem Phys 1939;7:1103.
[12] Alexander LE. X-ray diffraction method in polymer science. New York: Wiley-Interscience, 1969:137.
[13] Barham PJ, Keller A, Otun EL, Holmes PA. J Mater Sci 1984;19:2781.
[14] Visser JW. J Appl Cryst 1969;2:89.
[15] Okamura K, Marchessault RH. In: Ramachandran GN editor. Conformation of biopolymers, vol. 2. New York: Academic Press, 1967:709.
[16] Yokouchi M, Chatani Y, Tadokoro H, Teranishi K, Tani H. Polymer 1973;14:267.
[17] Vonk CG, Pijpers P. J Polym Sci Polym Phys Ed 1985;23:2517.
[18] Vonk CG. J Appl Cryst 1971;4:340.
[19] Vonk CG. J Appl Cryst 1973;6:81.
[20] Vonk CG, Kortleve G. Kolloid Z Polym 1967;220:19.
[21] Vonk CG. J Appl Cryst 1975;8:840.
[22] Barham PJ. J Mater Sci 1984;19:3826.
[23] Pearce R, Brown GR, Marchessault RH. Polymer 1994;35:3984.
[24] Pizzoli M, Scandola M, Ceccorulli G. Macromolecules 1994;27:4755.
[25] Dubini Paglia E, Beltrame PL, Canetti M, Seves A, Marcandalli B, Martuscelli E. Polymer 1993;34:996.
[26] Gazzano M, Tomasi G, Scandola M. Macromol Chem Phys 1997;198:71.
[27] Vonk CG. Makromol Chem; Macromol Symp 1988;15:215.